RSC Advances

PAPER

View Article Online
View Journal | View Issue

Cite this: *RSC Adv.*, 2018, **8**, 4329

Visible light photocatalytic mineralization of 17α-ethinyl estradiol (EE2) and hydrogen evolution over silver and strontium modified TiO_2 nanoparticles: mechanisms and phytotoxicity assessment†

Xueyu Wei, *[a] Jie Li,[b] Zhigang Liu,[e] Xiaofan Yang,[a] Saraschandra Naraginti,[c] Xiaoping Xu*[a] and Xiaoju Wang[d]

This study focusses on the novel synthesis of silver and strontium modified TiO_2 nanocomposite through a sol–gel method, which was then utilized for visible light degradation of EE2 and hydrogen production for the first time. Results indicated that co-doping of strontium and silver in the lattice of TiO_2 could remarkably narrow the band gap (2.89 eV) for efficient visible light activity, as indicated by UV-DRS, PL and photocurrent experiment results. The obtained nanocomposite was further characterized by various techniques including XRD, TEM, and XPS analysis. Furthermore, the well characterized photocatalyst was investigated for the photocatalytic hydrogen evolution under visible light irradiation. The hydrogen production rate of double atom doped TiO_2 (Sr/Ag–TiO_2, 49.4 μmol h^{-1}) is 2.6 times higher than that of single atom dopant (Ag–TiO_2, 19.6 μmol h^{-1}) nanocomposite. The plausible degradation pathway of EE2 during the photocatalytic process was investigated by LC-ESI/MS analysis. Additionally, to understand the toxicity of degraded metabolites and EE2, phytotoxicity testing was carried out on two common seeds, *V. radiata* and *P. vulgaris*., and 30% and 40% germination rate was noticed for seeds exposed to 50 ppm concentration of EE2 in *V. radiata* and *P. vulgaris* respectively, while 100% was noticed in seeds exposed to degraded metabolites, which revealed the less toxic nature of degraded metabolites compared to pure EE2. In addition, substantial growth rate was also observed in the roots and shoots of the seeds treated with the degraded metabolites compared to pure EE2. Therefore, the present study demonstrates the detoxification of EE2 and evolution of hydrogen under visible light, and would greatly help in evaluation and extenuation of the environmental risk of EE2 for water reuse and the generation of clean energy.

Received 21st November 2017
Accepted 7th January 2018

DOI: 10.1039/c7ra12638g

rsc.li/rsc-advances

Introduction

Hydrogen is a high energy density gas which has been described as a potential energy source for many green energy 'environmentally friendly' technologies. Statistical reports on energy necessitate the development and utilization of low price earth abundant materials as suitable materials for renewable energy technologies. However, these kinds of materials have some inadequate properties compared to that of currently existing efficient materials. These requirements may be fulfilled by titanium based compounds, since titanium is the ninth most abundant element in the earth's crust and the seventh most abundant metal. Titanium dioxide (TiO_2) is a well-known photocatalytic material with its high stability, non-toxicity, low cost and high performance in the mineralization of organic pollutants present in air and water.[1,2] However, TiO_2 catalysts are effective under UV irradiation, due to its high band gap (~3.2 eV), restricting the use of TiO_2 in practical applications since the UV region falls within 5% of total solar light spectrum. This urges researchers to develop facile modified materials to utilize the photocatalytic activity of the material in the visible region of solar spectrum. Modifying TiO_2 lattice by introducing other elements through physical and chemical processes, has been found to be a useful approach to obtain visible light sensitized catalysts which can initiate the water splitting mechanism.[3] Co-doping with two different atoms into TiO_2/ZnO matrices has attracted significant attention since they can exhibit higher photo-catalytic activity and unique

[a]*The School of Civil Engineering and Architecture, Anhui Polytechnic University, Wuhu – 241000, P. R. China. E-mail: wxyu1027@126.com; xuxp1979@126.com*

[b]*Jiangsu Academy of Environmental Industry and Technology Co Ltd, Nanjing – 210036, P. R. China*

[c]*Biofuels Institute, School of the Environment, Jiangsu University, 301 Xuefu Road, Zhenjiang – 212013, PR China*

[d]*School of Civil Engineering, Chongqing Three Gorges University, Wanzhou – 404000, P. R. China*

[e]*Ningbo Water Supply Co Ltd, Ningbo – 315041, P. R. China*

† Electronic supplementary information (ESI) available. See DOI: 10.1039/c7ra12638g

characteristics compared to doping them with a single element.[4–7] However, these metal dopants have to be used in small quantities to prevent recombination of photo-generated electrons and holes.[8] Thus, low concentration co-doping of cations and anions could be an effective solution to enhance the visible light absorption efficiency and also to reduce the recombination of the photo-generated charges.

The greater production and usage of pharmaceuticals (~4000 types of 100–200 000 tons per year) are the major reason for their increased levels of contaminants in water all over the world.[9] The pharmaceuticals that are enforced and consumed by humans and animals, which are further excreted and finally land up in wastewater treatment plants (WWTPs). Hence, it is an urge to reduce these pharmaceutical contaminants, because they can be very toxic to the ecosystems although they present in very low concentrations (ppb). These active pharmaceutical ingredients (APIs) are deliberately made to be static in which to remain biologically active with the aim of being effective in health care. Therefore, the remnants of these pharmaceuticals are very hard to treat by conventional methods in WWTPs, since only a fraction of them are being destroyed in the process.[10] On account of this, large amounts of these pharmaceutical pollutants were detected in aquatic environments and even in drinking water during the past years. These emerging contaminants were declared by US EPA as chemical compounds which are not regulated properly and whose effect on the environment and human health is poorly understood yet.[11] 17α-Ethinylestradiol (EE2) is a synthetic estrogen and endocrine-disrupting chemical (EDC) which is ranked in the top 100 of priority PPCPs.[12] 17α-Ethinylestradiol is one of the major components in contraceptive pills and postmenopausal hormonal appurtenances. By means of its removal during the treatment, EE2 is more resistant than other normal estrogen due its complicated chemical nature.[13] Often EE2 is also found in wastewater treatment plants (WWTPs) and is discharged into receiving waters due to its incomplete removal during the treatment process.[14] EE2 can induce the feminization in male fish and distort the reproductive potential and reduce the fish population even at trace levels of concentration.[15] Adverse effects on ecosystems, human health and drinking water safety, and its inefficient removal from WWTPs, it urges to explore effective techniques for EE2 removal within WWTPs.

Heterogeneous photocatalysis with visible light irradiation of metal modified TiO_2 nanoparticles has come forth as an effective technology for hydrogen generation and degradation of many pharmaceuticals,[16–18] for water reuse in agriculture and energy generation. The doping of two different atoms into TiO_2 lattice has attracted significant interest since it can exhibit higher photo-catalytic activity and unique characteristics compared to doping with a single element in visible light.[19,20] Through electron trapping, Ag and Sr doping could possibly inhibit the recombination of electrons and positive holes. Furthermore, Sr is one of the widely available alkaline earth metals exhibiting good electrical properties on doping with other metal oxides.[21,22] The present study deals with Ag and Sr modified TiO_2 nanoparticles for effective degradation of EE2 and hydrogen generation under visible light. The possible degradation pathway was investigated by HPLC and LC-ESI/MS analysis. Water reuse necessitates the phytotoxicity assessment of EE2 and their corresponding degradation metabolites. Hence, the phytotoxicity of the degraded metabolites and EE2 was investigated upon two common plant seeds *P. vulgaris* and *V. radiata* to insure the environmental impact of the treated water.

Materials and methods

Chemicals

Titanium(IV) isopropoxide, silver nitrate, strontium nitrate, 2-propanol, tween 20, hydrazine hydrate, 17α-ethinylestradiol (EE2), from Alibaba chemicals used in the present work were analytical grade reagents and used without further purification, millipore water was used in all experiments.

Synthesis of Ag and Sr modified TiO_2 nanoparticles

Metal modified TiO_2 nanoparticles (Ag/Sr–TiO_2) were prepared by sol–gel synthesis. In brief, a mixture of 5 mL of titanium(IV) isopropoxide and 50 mL isopropanol was added drop-wise to 200 mL of distilled water maintained pH ~ 1.5 while stirring. To the above solution required amounts of aqueous solutions of $AgNO_3$ and Sr $(NO_3)_2$ (0.2 mol% to 1.0 mol%) were added drop-wise under stirring. A small aliquot of distilled water and 50 mmol hydrazine hydrate were added to it followed by 5 mL of tween 20 and stirred for 30 min. The resultant sol was sonicated at 80 MHz for 90 min and then dried at 100 °C in a hot air oven for 24 h to get the dry gel which was calcined at 400 °C for 5 h to get the desired nanoparticles powder.

Photocatalytic degradation experiments

A laboratory scale photoreactor with Xe lamp (300 W) (emission spectrum shown in Fig. S1†) and a filter ($\lambda \leq 420$ nm) was used for visible light photocatalytic degradation experiments as shown in Fig. 1. In the photocatalytic experiments, 50 mL of the EE2 aqueous solution (10 mg L^{-1}) containing 50 mg of photocatalyst samples were first ultrasonicated, and then stirred in the dark for 1 h to ensure absorption–desorption equilibrium.[23,24] A small aliquot of the sample was collected at regular intervals and analyzed in HPLC during the photocatalytic irradiation for 6 h.

Photocatalytic hydrogen generation experiments

The photocatalytic hydrogen generation tests were carried out in a quartz reactor (180 mL) equipped with a loading port, sealed with a gas-tight rubber septum. 50 mg of the photocatalyst was dispersed by magnetic stirrer in 80 mL of aqueous solution containing 0.5 M Na_2S and 0.5 M Na_2SO_3 solution. The suspension was sonicated for 10 min before irradiation and purged with nitrogen gas for 30 min in order to remove all air in solution and headspace to ensure the reactor was in an anaerobic condition. 300 W Xe lamp with a filter ($\lambda \leq 420$ nm) was used to irradiate the sample for 5 h. The generated H_2 gas was collected at regular time intervals and analysed using an offline Shimadzu GC-2014 gas chromatograph (GC), equipped with a thermal conductivity detector (TCD) with a molecular sieve (5 Å) column, at 70 °C, using N_2 as the carrier gas. Control and the

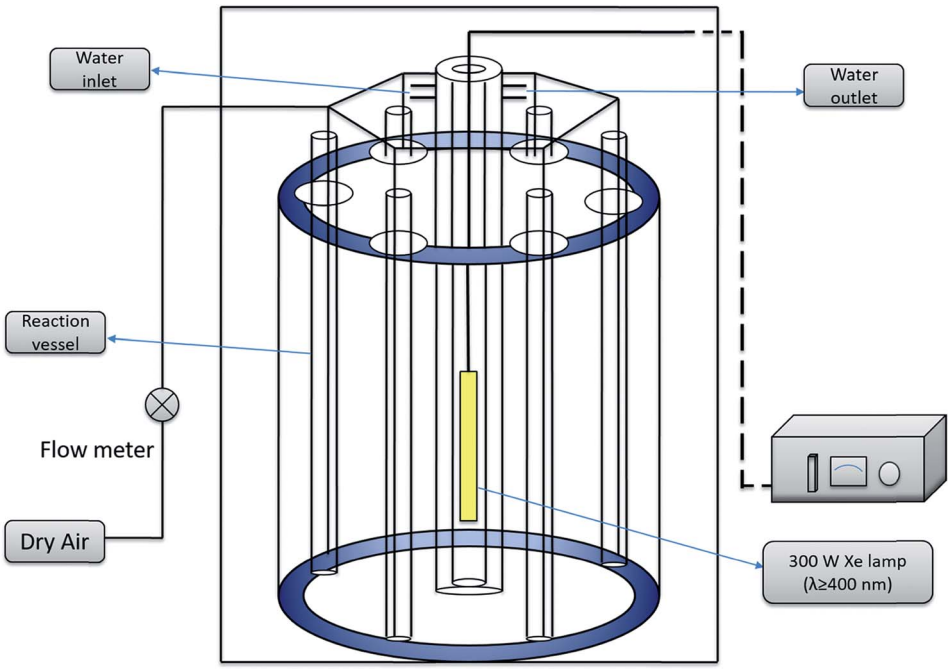

Fig. 1 Reactor set up for photocatalytic degradation of EE2.

blank (without catalyst) experiments were carried out under identical conditions for comparison.

Analytical methods

The remnant concentration of EE2 was determined using High Performance Liquid Chromatography (HPLC) technique. Agilent 1260 series with Eclipse XDBC18 (5 μm) reverse phase column (4.6 × 150 mm) was used for the separation. A fluorescence detector with an excitation wavelength of 280 nm and an emission wavelength of 310 nm was used in this study.[25] The mobile phase with a mixture of water and methanol (30 : 70 v/v) was used with an injection volume of 1 mL min^{-1} for 6 minutes. The analysis of EE2 degradation metabolites was carried by liquid chromatography tandem mass spectrometry (Agilent 1290 Infinity Binary LC system, Agilent 6460 Triple Quadrupole LCMS/MS system employing the Zorbax eclipse plus C18 column; rapid resolution, 2.1 × 50 mm, 1.8 μm). The mobile phase of methanol and water at 30 : 70 (v/v) was used for EE2 about 60 min. To obtain mass spectra electro spray ionization (ESI) was used under the flow of helium gas at approximately 1 mL min^{-1} and 16 V of fragment voltage.

Photoelectrochemical measurements

The electrochemical measurements were carried out in a three-electrode quartz cells using CHI760B as an electrochemical workstation. Pt wire as the counter electrode and saturated calomel electrodes (SCE) as the reference electrode was used during the measurements. For the working electrode typically

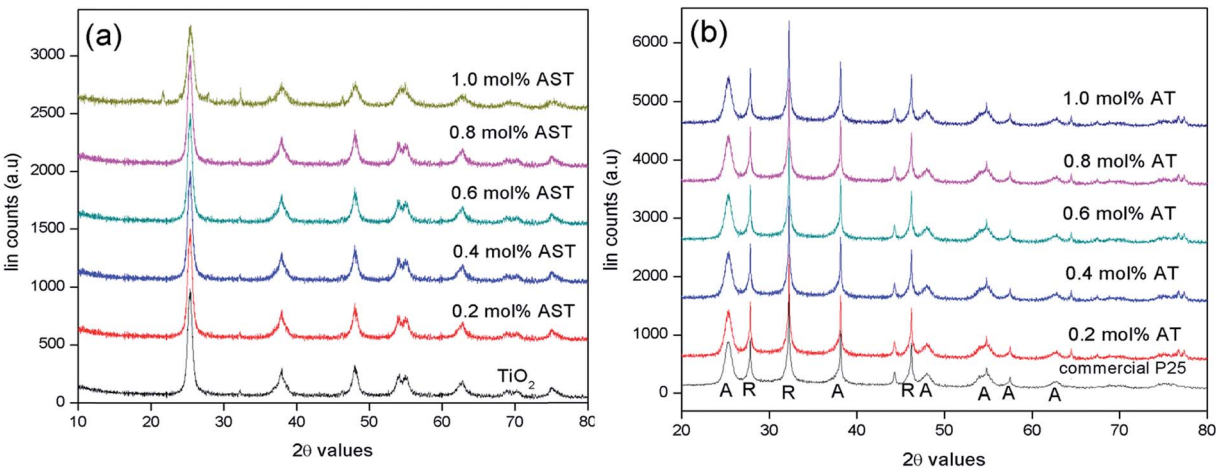

Fig. 2 X-ray diffraction pattern of synthesized (a) Sr/Ag–TiO_2 and (b) Ag–TiO_2 nanoparticles.

5 mg of the photocatalyst was dissolved in 1.0 mL of DMF solution and sonicated for 10 min, then 20 μL of the suspension was dropped on FTO with an fixed area of 0.5 cm^2, and then dried at ambient temperature for 24 h to form photocatalysts modified FTO. For light source 500 W Xe arc lamp was utilized in the photoelectrochemical measurements.

Characterization of nanoparticles

X-ray diffraction patterns of the synthesized nanoparticles were recorded on BRUKER D8-Advance X-ray diffractometer with Cu Kα source ($\lambda = 1.5406$ Å). TEM imaging and EDS analysis were recorded on JEOL JEM 2100 high resolution transmission electron microscope (HRTEM). Diffused reflectance spectra were recorded with a JASCO V-670 UV-vis spectrophotometer. The photoluminescence (PL) spectra were obtained on a HITACHI F-7000 fluorescence spectrophotometer. XPS data was acquired with a Kratos Axis Ultra 165 Spectrometer with a monochromated Al Kα X-ray source ($h\alpha = 1486.6$ eV).

Phytotoxicity test

The phytotoxicity test was carried out on two common crop seeds *P. vulgaris* and *V. radiata* for EE2 and its corresponding degradation metabolites products (50 mg L^{-1}) generated during photocatalytic degradation process. Ethyl acetate was used to extract the degradation metabolites of EE2, the extract was dried and dissolved in 10 mL of distilled water to make a final concentration of 50 ppm. The phytotoxicity assessment test was carried out systematically based on the prescribed guidelines in the literature[26,27] with minor modifications. From each type of plant variety 10 seeds were sterilized using 1–5% sodium hypochlorite solution for 15 min, and then rinsed thoroughly with distilled water to ensure complete removal of sodium hypochlorite from the surface of the seeds. Seeds were then immersed with EE2 (50 ppm) and the degradation metabolites (50 ppm) solutions in 100 mL Erlenmeyer flasks separately. Seeds immersed in distilled water were included beside as control. After interaction was finished, the all 10 seeds were placed on wet cotton in Petri dish and incubated at 25 ± 1 °C in dark for 24 h. Only germinated seeds were picked out for further phytotoxicity analysis. Further test was conducted in standard beakers contains 50 ppm of EE2 and its degradation metabolites dissolved in 30 mL of 1.5% of agar. The beakers were kept in freezer for few minutes to harden agar media immediately. The germinated seedlings were then placed on the surface of the agar in each beaker and incubated at 25 ± 1 °C in darkness. After 7 days of incubation the plants were separated from the

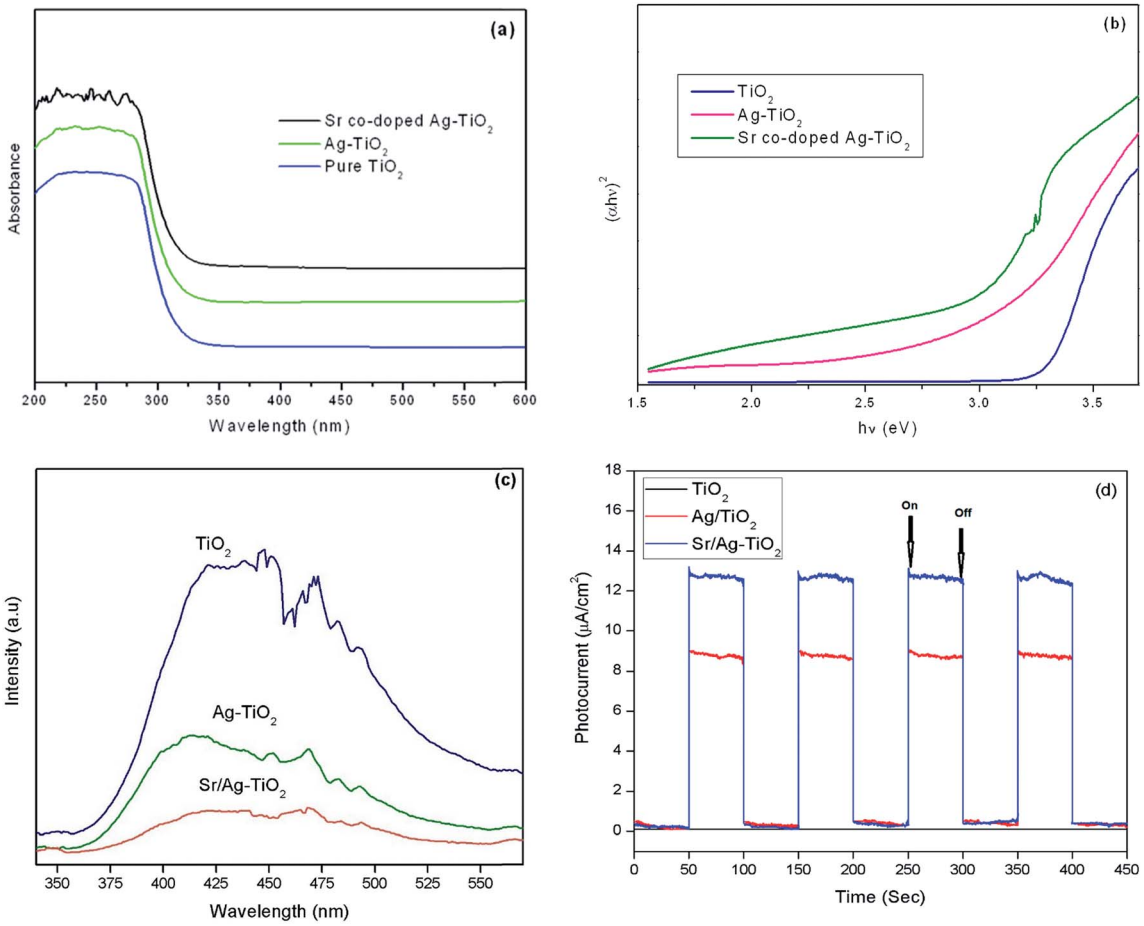

Fig. 3 (a) UV-vis DRS spectra, (b) optical energy band gap spectra (E_g), (c) photoluminescence and (d) photocurrent response of the prepared nanoparticles.

agar and lengths of root and shoot was measured. All the experiments were carried out in triplicate and average data was reproduced in the present study.

Results and discussion

Characterization of nanoparticles

Fig. 2a shows X-ray diffraction pattern of Sr/Ag–TiO_2 nanoparticle which was supported by anatase phase with the 2θ peaks at 25.3°, 37.9°, 47.9°, 55.0° and 62.8° respectively. All the values are completely matched with standard anatase phase TiO_2, however mixed phase (anatase and rutile) was observed in Ag doped TiO_2 (Fig. 2b) samples. Due to lower concentrations of dopant no signals were observed corresponds to Ag and Sr in XRD patterns, this could be revealed that doping of metal atoms into TiO_2 did not alter its phase crystallinity.

The UV-vis absorption spectra of pure TiO_2, Ag/TiO_2 and Sr/Ag–TiO_2 are shown in Fig. 3a. The red shift in absorption band from 350 nm to 400 nm could be due to the photo-excitation occurring at valence band to conduction band. TiO_2 nanoparticles modified with single atom (silver) has lower shift in comparison to two atoms (strontium and silver, 1.0 mol%). Kubelka Munk extrapolation plot of $h\nu$ *vs.* $(\alpha h\nu)^2$ was used to get optical energy band gap values (E_g) as depicted in Fig. 3b. These values for TiO_2, Ag/TiO_2 and Sr/Ag–TiO_2 nanoparticles were found to be about 3.17 eV, 3.06 eV and 2.89 eV respectively. It revealed that the titanium dioxide modified with two atoms (silver and strontium) was followed with a decrease in the band energy and an increase in the wave length. Further to understand the stability and recombination of photogenerated electron photoluminescence (PL) study was carried out (Fig. 3c). The PL spectra of the doped and undoped TiO_2 are shown near band gap emission (NBE) and blue or deep level emission. These results suggest that the quelling of NBE on doping TiO_2 with silver and strontium, which may be due to the inhibition of recombination of the photogenerated electron–hole pairs on doped TiO_2. Fig. 3d shows the photocurrent response of the synthesised TiO_2, Ag/TiO_2 and Sr/Ag–TiO_2 nanoparticles. Upon visible light irradiation, the photocurrent rapidly increases and reaching a platform. The photocurrent of Sr/Ag–TiO_2 was higher than that of Ag/TiO_2 and TiO_2 nanoparticles, suggesting

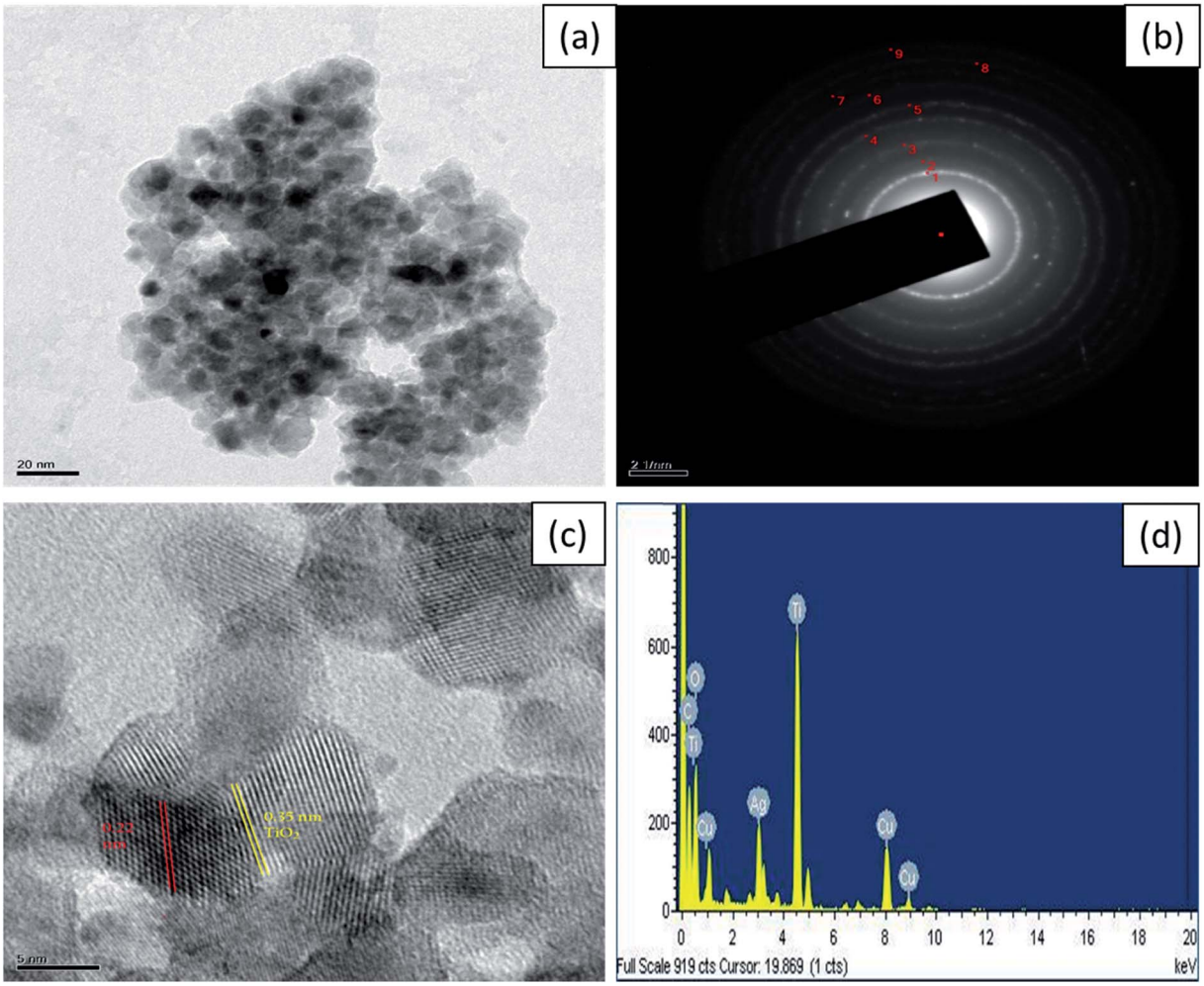

Fig. 4 TEM images (a) and (b), selected area electron diffraction pattern (c), EDS profile (d) showing the elements present in the prepared Ag–TiO_2 nanoparticles.

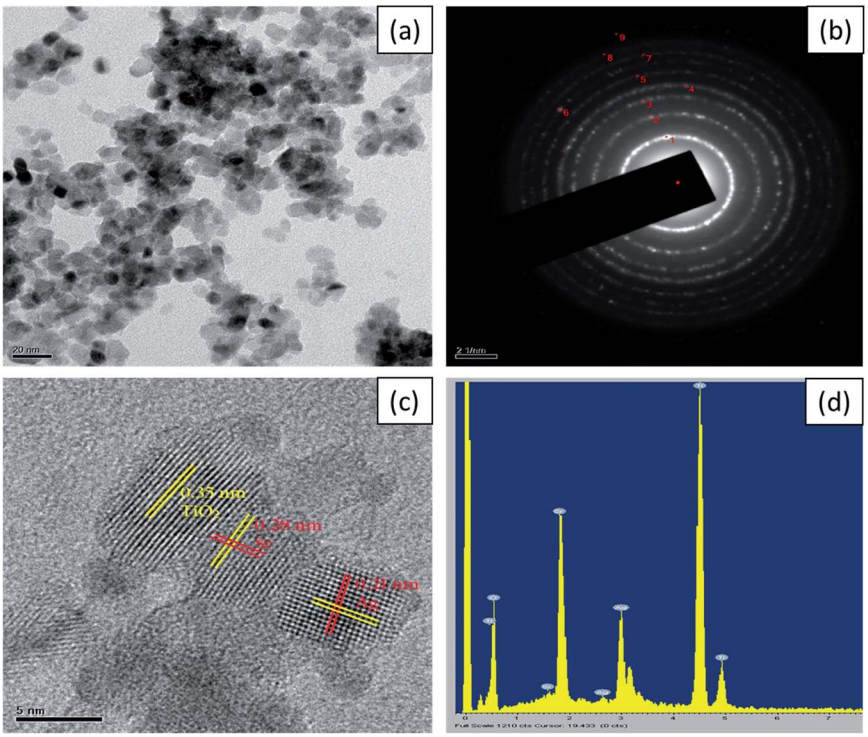

Fig. 5 TEM images (a) and (b), selected area electron diffraction pattern (c), EDS profile (d) showing the elements present in the prepared Sr/Ag–TiO_2 nanoparticles.

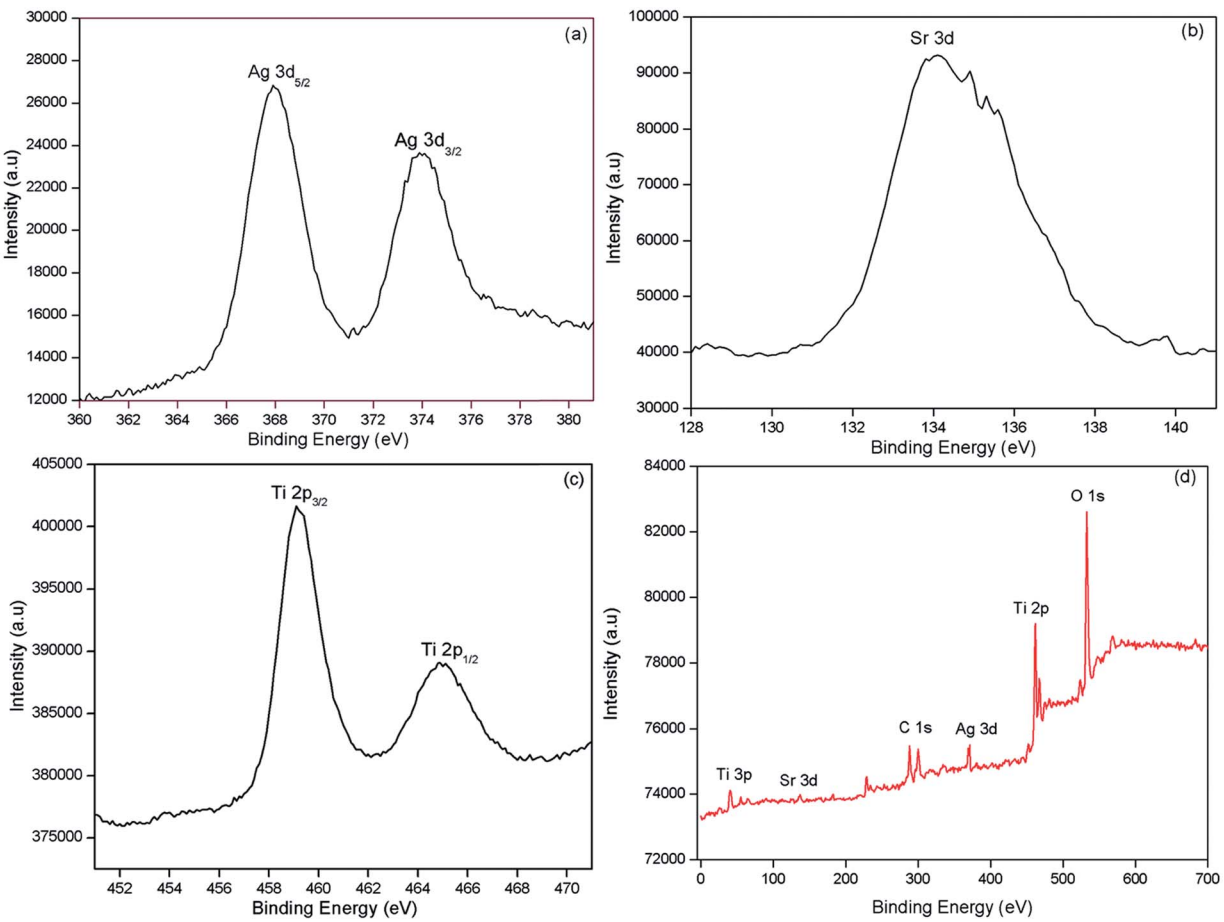

Fig. 6 High resolution XPS spectra of Ag 3d (a), Sr 3d (b), Ti 2p (c) orbitals and broad XPS spectrum (d) of Sr/Ag–TiO_2 nanocomposite.

a higher separation efficiency of photogenerated charge carriers.[28]

The TEM images of Ag/TiO_2 (Fig. 4a) and Sr/Ag–TiO_2 (Fig. 5a) nanoparticles indicate that the particles are ranges from 7 to 22 nm and 13 to 31 nm respectively. The SAED pattern of this samples are shown in Fig. 4b and 5(b), in which the dark rings on the right correspond to the standard polycrystalline diffraction rings for the anatase phase (indexed). High resolution TEM images (Fig. 4c and 5c) were obtained to understand more evident microstructure information of the nanoparticles to enable accurately analyzes the single grains and grain boundaries. EDS spectrum (Fig. 4d and 5d) indicates elemental compositions that are present in the TiO_2 support.

In order to confirm the chemical state and surface composition XPS analysis was carried out for Sr/Ag–TiO_2 nanoparticles. The apparent XPS scans of Ag 3d, Sr 3d, Ti 2p and O 1s levels are executed to understand whether the dopant Ag and Sr atoms are interlinking in the lattice of TiO_2 or react with Ti and O to form other compounds. Fig. 6a shows high-resolution XPS spectrum of Ag at 3d core levels, indicates that the Ag $3d_{5/2}$ and Ag $3d_{3/2}$ binding energies are observed at 368.1 and 374.1 eV respectively, which are corresponded to metallic silver.[29,30] The Sr 3d core level peak was observed at 133.7 was in complete agreement with the literature (Fig. 6b).[31,32] The binding energies of Ti $2p_{3/2}$ and Ti $2p_{1/2}$ (Fig. 6c), photoelectron peaks was observed at 459.2 and 464.9 eV respectively.[33,34] The broad spectrum of Sr/Ag–TiO_2 nanocomposite was shown in Fig. 3d, indicated that silver, titanium and strontium metal ions were present in their highest oxidation state. The presence of Ag and Sr in broad XPS spectrum and detection of no new compounds between Ag, Sr, O, and Ti atoms, may confirm that Ag and Sr atoms were doped into TiO_2 crystal lattice.

Photocatalytic hydrogen generation

In order to determine the photocatalytic performance of the synthesized photocatalysts, hydrogen evolution experiments were carried out under visible light irradiation in the presence of Na_2S (0.5 M) and Na_2SO_3 (0.5 M) solution. From the Fig. 7a,

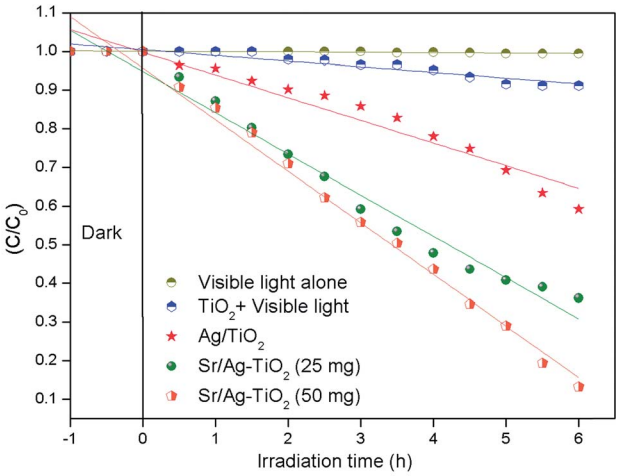

Fig. 8 Degradation kinetics of EE2 under visible light irradiation at different time intervals using Sr/Ag–TiO_2 nanoparticles.

from H_2 evolution kinetic curves shows that the amount of H_2 increases with the irradiation time by the visible light ($\lambda \geq 420$ nm). The results indicate that TiO_2 nanoparticles modified with Ag and Sr show efficient photocatalytic hydrogen generation activity as compared to their single components of Ag–TiO_2, and TiO_2. Further, the Ag and Sr modified TiO_2 nanoparticles shown the highest hydrogen production activity. Fig. 7b indicates the average hydrogen production rates of as-obtained samples. Obviously no noticeable H_2 was generated for pure TiO_2 under visible light irradiation. The hydrogen production rate on Ag–TiO_2 is low, which is only 19.6 μmol per one hour, while the hydrogen production rate of Sr/Ag–TiO_2 is 49.4 μmol h^{-1}. These production rates are 2.6 times higher than that of Ag–TiO_2 nanocomposite. These results suggest that the hydrogen production rate of TiO_2 is remarkably enhanced by doping silver and strontium ions in the TiO_2 crystal lattice. The enhanced H_2 evolution activity of Sr/Ag–TiO_2 also attributed by the heterojunction electric field among the TiO_2, silver and strontium atoms and visible light

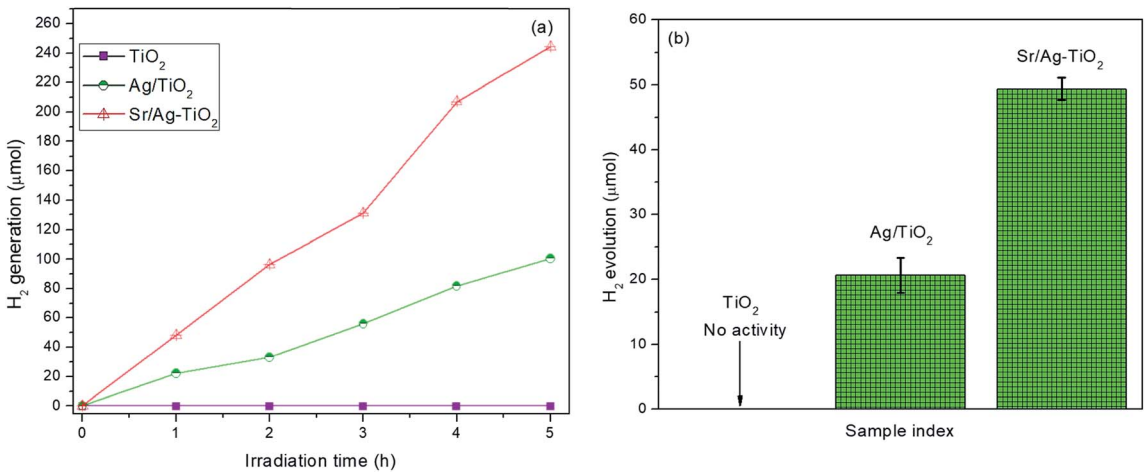

Fig. 7 (a) Time dependant photocatalytic H_2 evolutions and (b) average hydrogen production rates.

harvesters of Ag and Sr (narrow bandgap).[35,36] As described in UV-vis DRS section, upon visible light irradiation on the surface of the catalysts, the photo-generated electrons in the CB of Ag and Sr tends to transfer to the CB of TiO_2, meanwhile the holes in the VB of Ag and Sr will move to the VB of TiO_2. With this process, the photo-induced carriers within this ternary system can be successfully separated as supported by the PL studies and photocurrent results, thus excellent photocatalytic activity can be achieved. The pertinent series of reactions at the surface of the semiconductor causing the hydrogen generation and pollutant degradation can be expressed as follows:

$$Sr/Ag\text{–}TiO_2 + h\nu \rightarrow e^- + h^+ \quad (1)$$

$$h^+ + H_2O \rightarrow {}^{\cdot}OH + H^+ \quad (2)$$

$$2H^+ + 2e^- (CB) \rightarrow H_2 \quad (3)$$

$$H^+ + OH^- (VB) \rightarrow {}^{\cdot}OH \quad (4)$$

$$O_2 + e^- \rightarrow O_2^{\cdot -} \quad (5)$$

EE2 + $^{\cdot}OH$ and $O_2^{\cdot -}$ → degradation metabolites

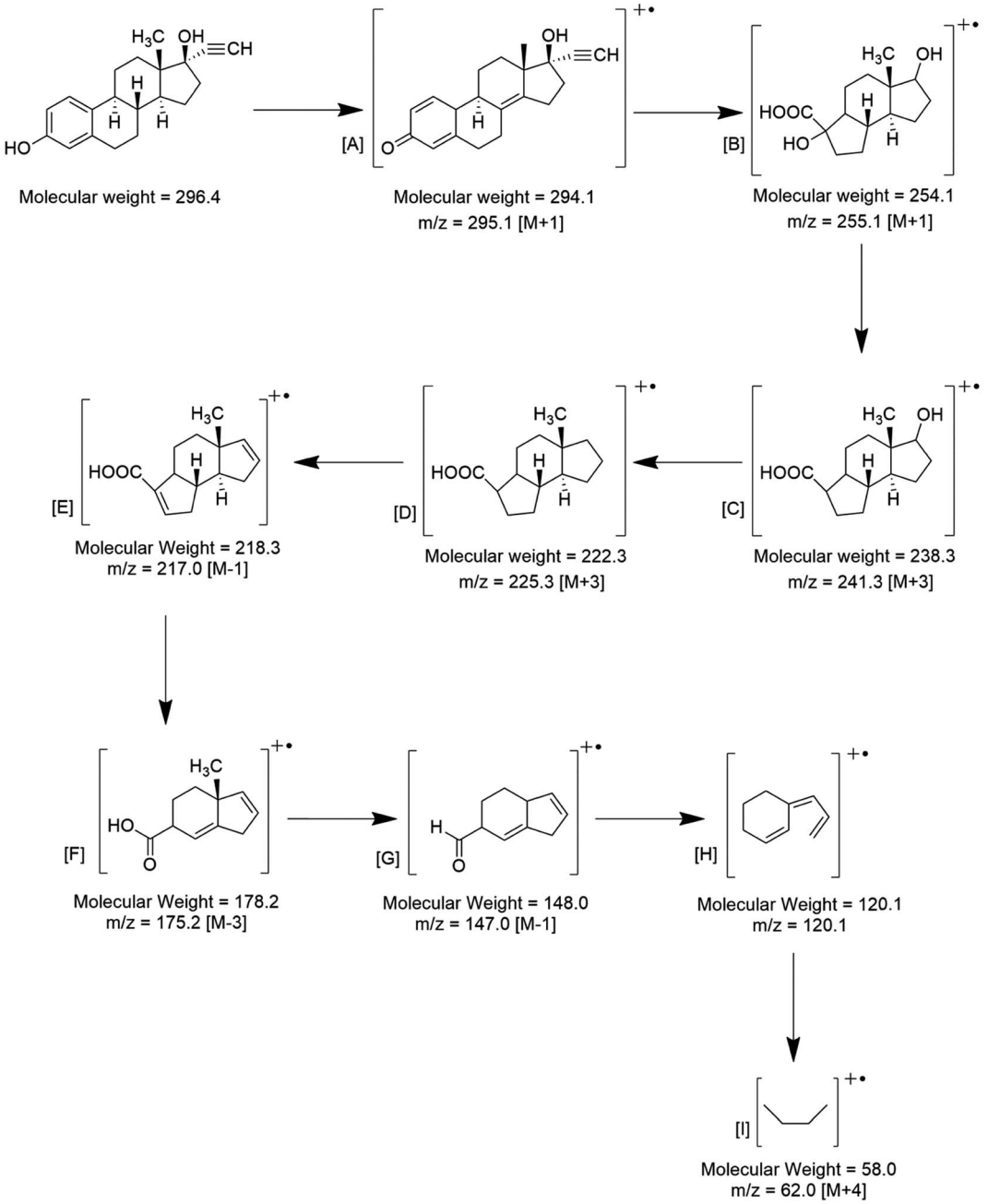

Fig. 9 Plausible degradation pattern of EE2 under visible light irradiation using Sr/Ag–TiO_2 nanoparticles.

Table 1 Phytotoxicity assessment of EE2 and their corresponding extracted intermediates (after 7 days of incubation)[a]

	Vigna radiata			*Phaseolus vulgaris*		
	Germination (%)	Shoot (cm)	Root (cm)	Germination (%)	Shoot (cm)	Root (cm)
Water	100	9.87 ± 0.57**	5.47 ± 0.63	100	7.15 ± 1.31	2.17 ± 0.54*
EE2	50	2.90 ± 0.31*	1.02 ± 0.17	50	2.98 ± 0.83**	1.15 ± 0.17
EE2 metabolites	100	4.95 ± 0.51*	2.12 ± 0.24**	100	5.75 ± 0.40*	1.56 ± 0.25*

[a] Values are mean of germination seeds treated with SMX, RR-194 and degraded metabolites, significantly different from the seeds germinated with tap water at*$P < 0.05$, **$P < 0.01$, by one-way analysis of variance (ANOVA).

Photocatalytic degradation of 17α-ethinyl estradiol

The photocatalytic degradation kinetics of EE2 can be depicted by a Langmuir–Hinshelwood model (eqn (1)), which exemplified that the reactions took place at a solid–liquid interface.

$$\ln[C_o/C_t] = k_r K_t = K_{apr} t \quad (6)$$

The plot of $\ln(C_0/C)$ *versus* the irradiation time with various photocatalysts in 6 h under visible light irradiation is shown in Fig. 8. The results indicated that degradation of EE2 follows first-order kinetics because the regression coefficients (R^2) are all above 0.8856. Apparently, in all the tested photocatalysts for degradation of EE2, Sr/Ag–TiO_2 nanocomposite was found to be the best performance with rate constant k = 0.1699 min^{-1}.

To further investigate the plausible degradation pathway of EE2 during visible light irradiation LC-ESI/MS analysis was performed over visible light irradiated Sr/Ag–TiO_2 nanoparticles. LC-MS analysis of the EE2 degraded samples evidenced the presence of compounds with molecular weights 294.1, 254.1, 238.3, 222.3, 218.3, 178.2, 148.0, 120.1 and 58.1 which could be interpreted as (M+), (M+), (M + 3), (M + 3), (M − 1), (M − 3), (M − 1), (M) and (M + 4) peaks of structure A, B, C, D, E, F, G, H and I (Fig. 9, S2 and S3†).

Further to investigate the stability and recycle photocatalytic performance of the as-prepared Sr/Ag–TiO_2 nanoparticles, photocatalytic degradation of EE2 is cycled for four times and the results are shown in Fig. S4.† After each run, the photocatalyst was recycled by centrifuging, washing, and drying and was used for the next run. As can be seen from the results, no obvious decrease in photocatalytic degradation performance can be found after four cycles (94%), which demonstrates that the Sr/Ag–TiO_2 nanoparticles have high photocatalytic stability and excellent reusability.

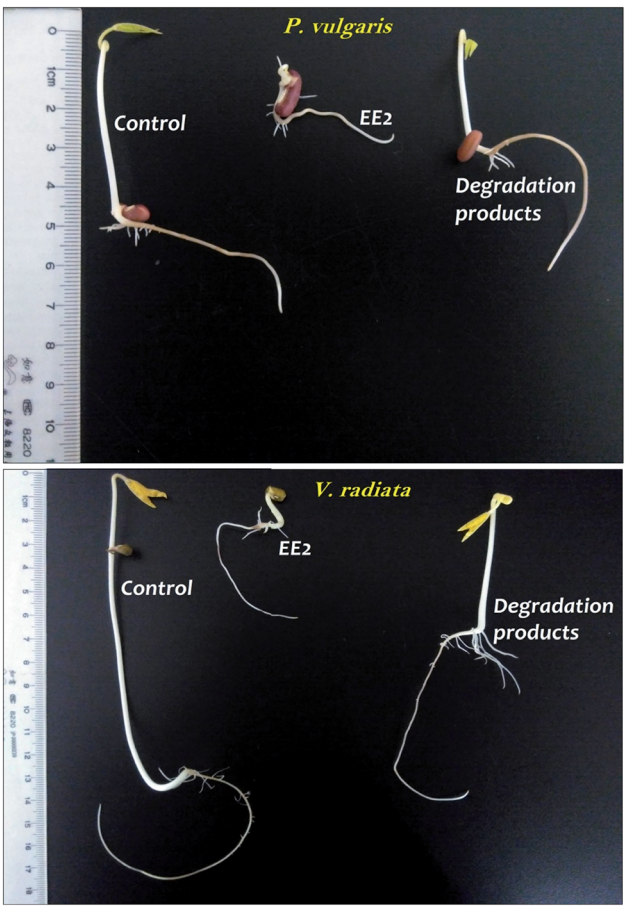

Fig. 10 Phytotoxicity assessment of EE2 and its visible light degradation products.

Phytotoxicity test

The disposal of the untreated/partially treated effluents of EDCs not only causes severe environmental and health hazards but also has a direct impact on the soil, affecting its fertility. This necessitates the assessment of phytotoxicity of EDCs and its corresponding degraded metabolites. 17α-ethinyl estradiol (50 ppm) highly inhibited the germination rate of *P. vulgaris* and *V. radiata*, reducing it to 50%. Interestingly, seeds exposed to 50 ppm of the photocatalytic degradation products and distilled water (control) exhibited 100% germination rate in both the types of seeds. Furthermore, EE2 also showed its toxicity on the length of root and shoots of the plants. In the case of *P. vulgaris* the shoot and root lengths are 2.98 ± 0.83 and 1.15 ± 0.17 respectively. Similarly, in the case of *V. radiata* the shoot and root lengths are found to be 2.90 ± 0.31 and 1.02 ± 0.17 respectively. In contrast to this higher shoot and root lengths were observed in the case of seeds grown in degraded products as well as in control (Table 1) and (Fig. 10). Thus, these results of phytotoxicity test indicated the ability of the prepared nanoparticles to not only degrade toxic pollutant EE2 but also to detoxify it.

Conclusions

Novel metal modified TiO_2 nanoparticles were synthesized and used in the photocatalytic degradation of 17α-ethinyl estradiol under visible light and generation of hydrogen. The production rate of H_2 for double atom doped TiO_2 (Sr/Ag–TiO_2) is 2.6 times higher than that of single atom dopant (Ag–TiO_2). Further the plausible transformation pathway of EE2 and degradation products were determined by LC/ESI-MS analysis. According to phytotoxicity assessment it is suggested that the degraded products induces better growth in root and shoots compare to pure 17α-ethinyl estradiol in *P. vulgaris*, and *V. radiata*, which evidenced that less toxic intermediates were generated during visible light degradation process. Thus, we conceive that the present study provides the ability of multifunctional nanomaterials of Sr/Ag–TiO_2 to simultaneously degrade and detoxify the contaminated water and also utilized for energy generation during photocatalysis.

Conflicts of interest

There are no conflicts to declare.

Acknowledgements

This study was supported by the Natural Science Key Foundation of Education Committee of Anhui Province (No. KJ2016A063 and No. KJ2017A119), the Fundamental Research Funds for the Central Universities (No. 2016B44014), the Natural Science Foundation of China (No. 51502106).

References

1 H. Q. Sun, S. B. Wang, H. M. Ang, M. O. Tadé and Q. Li, *Chem. Eng. J.*, 2010, **162**, 437–447.
2 J. W. Chen, J. W. Shi, X. Wang, H. Y. Ai, H. J. Cui and M. L. Fu, Hybrid metal oxides quantum dots/TiO_2 block composites: facile synthesis and photocatalysis application, *Powder Technol.*, 2013, **246**, 108–116.
3 W. Zhao, W. H. Ma, C. C. Chen, J. C. Zhao and Z. G. Shuai, *J. Am. Chem. Soc.*, 2004, **126**, 4782–4783.
4 X. Zhou, F. Peng, H. Wanga and H. Yu, *J. Solid State Chem.*, 2011, **184**, 3002–3007.
5 N. Zhao, M. Yao, F. Li and F. Lou, *J. Solid State Chem.*, 2011, **184**, 2770–2775.
6 X. Yanga, F. Mab, K. Li, Y. Guob, J. Hub, W. Li, M. Huoa and Y. Guob, *J. Hazard. Mater.*, 2010, **175**, 429–438.
7 H. Serier, O. Toulemonde, D. Bernard, A. Demourgues, J. Majimel and M. Gaudon, *Mater. Res. Bull.*, 2012, **47**, 755–762.
8 R. Dholam, N. Patel, M. Adami and A. Miotello, *Int. J. Hydrogen Energy*, 2009, **34**, 5337–5346.
9 L. M. P. Martínez, J. L. Faria, J. M. Do-na-Rodríguez, C. Fern_andez-Rodríguez and A. M. T. Silva, Degradation of diphenhydramine pharmaceutical in aqueous solutions by using two highly active TiO_2 photocatalysts: operating parameters and photocatalytic mechanism, *Appl. Catal., B*, 2012, **113–114**, 221–227.
10 R. Mohammadi, B. Massoumi and M. Rabani, Photocatalytic decomposition of amoxicillin trihydrate antibiotic in aqueous solutions under UV irradiation using Sn/TiO_2 nanoparticles, *Int. J. Photoenergy*, 2012, 1–11.
11 T. Deblonde, C. Cossu-Leguille and P. Hartemann, Emerging pollutants in wastewater: a review of the literature, *Int. J. Hyg. Environ. Health*, 2011, **214**(6), 442–448.
12 D. Nasuhoglu, D. Berk and V. Yargeau, Photocatalytic removal of 17α-ethinylestradiol (EE2) and levonorgestrel (LNG) from contraceptive pill manufacturing plant wastewater under UVC radiation, *Chem. Eng. J.*, 2012, **185**, 52–60.
13 S. Hwang, D. I. Lee, C. H. Lee and I. S. Ahn, Oxidation of 17α-ethinylestradiol with Mn(III) and product identification, *J. Hazard. Mater.*, 2008, **155**, 334–341.
14 Z. Zhang, Y. Feng, Y. Liu, Q. Sun, P. Gao and N. Ren, Kinetic degradation model and estrogenicity changes of EE2 (17α-ethinylestradiol) in aqueous solution by UV and UV/H_2O_2 technology, *J. Hazard. Mater.*, 2010, **181**, 1127–1133.
15 C. E. J. R. Desbrow, E. J. Routledge, G. C. Brighty, J. P. Sumpter and M. Waldock, Identification of estrogenic chemicals in STW effluent. 1. Chemical fractionation and *in vitro* biological screening, *Environ. Sci. Technol.*, 1998, **32**, 1549–1558.
16 N. Lakshmana Reddy, S. Kumar, V. Krishnan, M. Sathish and M. V. Shankar, Multifunctional Cu/Ag quantum dots on TiO_2 nanotubes as highly efficient photocatalysts for enhanced solar hydrogen evolution, *J. Catal.*, 2017, **350**, 226–239.
17 L. Gnanasekaran, R. Hemamalini, R. Saravanan, K. Ravichandran, F. Gracia and V. K. Gupt, Intermediate state created by dopant ions (Mn, Co and Zr) into TiO_2 nanoparticles for degradation of dyes under visible light, *J. Mol. Liq.*, 2016, **223**, 652–659.
18 Y. He, N. B. Sutton, H. H. H. Rijnaarts and A. A. M. Langenhoff, Degradation of pharmaceuticals in wastewater using immobilized TiO_2 photocatalysis under simulated solar irradiation, *Appl. Catal., B*, 2016, **182**, 132–141.
19 R. Aiswal, N. Patel, A. Dashora, R. Fernandes, M. Yadav, R. Edla, R. S. Varma, D. C. Kothari, B. L. Ahuja and A. Miotello, Efficient Co-B-codoped TiO_2 photocatalyst for degradation of organic water pollutant under visible light, *Appl. Catal., B*, 2016, **183**, 242–253.
20 Q. Guo, Z. Zhang, X. Ma, K. Jing, M. Shen, N. Yu, J. Tang and D. D. Dionysiou, Preparation of N,F-codoped TiO_2 nanoparticles by three different methods and comparison of visible-light photocatalytic performances, *Sep. Purif. Technol.*, 2017, **175**, 305–313.
21 S. Sood, A. Umar, S. K. Mehta, A. S. K. Sinha and S. K. Kansal, Efficient photocatalytic degradation of brilliant green using Sr-doped TiO_2 nanoparticles, *Ceram. Int.*, 2015, **41**, 3533–3540.
22 N. N. Kumaran and K. Muraleedharan, Photocatalytic activity of ZnO and Sr^{2+} doped ZnO nanoparticles, *Journal of Water Process Engineering*, 2017, **17**, 264–270.

23 A. Hernández-Gordillo and V. Rodríguez González, Silver nanoparticles loaded on Cu-doped TiO_2 for the effective reduction of nitro-aromatic contaminants, *Chem. Eng. J.*, 2015, **261**, 53–59.

24 E. B. Simsek, Solvothermal synthesized boron doped TiO_2 catalysts: Photocatalytic degradation of endocrine disrupting compounds and pharmaceuticals under visible light irradiation, *Appl. Catal., B*, 2017, **200**, 309–322.

25 Y. Yoon, P. Westerhoff, S. A. Snyder and M. Esparza, HPLC-fluorescence detection and adsorption of bisphenol A, 17β-estradiol, and 17α-ethynyl estradiol on powdered activated carbon, *Water Res.*, 2003, **37**, 3530–3537.

26 USEPA, *Ecological effects test guidelines. Seed germination root elongation toxicity test. Office of prevention, Pesticides and Toxic substances 850. 4200*, Washington DC, EPA 712-C-96–163, 1996.

27 A. S. Arun Prasad, V. S. V. Satyanarayana and K. V. Bhaskar Rao, Biotransformation of Direct Blue 1 by a moderately halophilic bacterium Marinobacter sp. strain HBRA and toxicity assessment of degraded metabolites, *J. Hazard. Mater.*, 2013, **262**, 674–684.

28 Z. Jiang, K. Qian, C. Zhu, H. Sun, W. Wan, J. Xie, H. Li, Po K. Wong and S. Yuan, Carbon nitride coupled with CdS-TiO_2 nanodots as 2D/0D ternary composite with enhanced photocatalytic H_2 evolution: A novel efficient three-level electron transfer process, *Appl. Catal., B*, 2017, **210**, 194–204.

29 E. Sumesh, M. S. Bootharaju, Anshup and T. Pradeep, A practical silver nanoparticle-based adsorbent for the removal of Hg^{2+} from water, *J. Hazard. Mater.*, 2011, **189**, 450–457.

30 Y. Lai, H. Zhang, K. Xie, D. Gong, Y. Tang, L. Sun, C. Lin and Z. Chen, Fabrication of uniform Ag/TiO_2 nanotube array structures with enhanced photoelectrochemical performance, *New J. Chem.*, 2010, **34**, 1335–1340.

31 H. A. Hamedani, N. K. Allam, H. Garmestani and M. A. El-Sayed, Electrochemical fabrication of strontium-doped TiO_2 nanotube array electrodes and investigation of their photoelectrochemical properties, *J. Phys. Chem. C*, 2011, **115**, 13480–13486.

32 S. Sood, A. Umar, S. K. Mehta, A. S. K. Sinha and S. K. Kansal, Efficient photocatalytic degradation of brilliant green using Sr-doped TiO_2 nanoparticles, *Ceram. Int.*, 2015, **41**, 3533–3540.

33 K. V. Bineesh, S. Y. Kim, B. R. Jermy and D. W. Park, Catalytic performance of vanadia-doped titania-pillared clay for the selective catalytic oxidation of H_2S, *J. Ind. Eng. Chem.*, 2009, **15**, 207–211.

34 Y. Kim, J. Lee, H. Jeong, Y. Lee, M. H. Um, K. M. Jeong, M. K. Yeo and M. Kang, Methyl orange removal over Zn-incorporated TiO_2 photo-catalyst, *J. Ind. Eng. Chem.*, 2008, **14**, 396–400.

35 C. Zhang, K. Yu, Y. Feng, Y. Chang, T. Yang, Y. Xuan, D. Lei, L.-L. Lou and S. Liu, Novel 3DOM-$SrTiO_3$/Ag/Ag_3PO_4 ternary Z-scheme photocatalysts with remarkably improved activity and durability for contaminant degradation, *Appl. Catal., B*, 2017, **210**, 77–87.

36 K. Yu, C. Zhang, Y. Chang, Y. Feng, Z. Yang, T. Yang, L.-L. Lou and S. Liu, Novel three-dimensionally ordered macroporous $SrTiO_3$ photocatalysts with remarkably enhanced hydrogen production performance, *Appl. Catal., B*, 2017, **200**, 514–520.